

## MODELLING OF FLAT-PLATE COLLECTORS BASED ON MONOLITHIC SILICA AEROGEL

A. NORDGAARD\* and W. A. BECKMAN\*\*

\* Norwegian Institute of Technology, University of Trondheim, Norway, \*\* Solar Energy Laboratory,  
University of Wisconsin, Madison, Wisconsin, U.S.A.

**Abstract**—This paper presents a new method for predicting the radiative transfer in an absorbing and isotropically scattering, non-gray plane-parallel atmosphere. The technique is based upon the  $\hat{F}$  ("F-hat") concept and was developed to determine the radiative transfer at short wavelengths for the transparent insulation material, monolithic silica aerogel. The angular dependence of solar transmittance of diffuse and ground reflected radiation is evaluated along with the "transmittance-absorptance product" of a collector. The  $\hat{F}$  technique is also used to determine the IR transmission of the cover from which the overall loss coefficient for a flat-plate collector constructed with aerogel filled covers is determined. The performance of a system using aerogel collectors is compared to systems using other types of high performing collectors. It is shown that, at least for the system investigated, the decrease in solar transmittance of monolithic silica aerogel is more than compensated by the decrease in thermal losses.

### 1. INTRODUCTION

It has been experimentally shown by Svendsen and Jensen [20] and Svendsen [21] that flat-plate collector efficiency can be significantly improved by filling the air gap between absorber and cover with monolithic silica aerogel (MSA), and evacuating the system to 0.1 bar. The most recent collector design proposed by Svendsen is illustrated in Fig. 1. The collector consists of a plain, black painted absorber made from copper tubes with copper foils on each side. The copper foils are supported by means of blocks of suitable material. Both sides and the edges of the absorber are covered by 20 mm thick MSA tiles and 4 mm tempered low-iron glass. A frame of stainless steel placed between the glass is sealed with butyl to make the collector box airtight. Although the construction is symmetric in order to reduce thermal stress problems and both sides could be illuminated, in this study only one surface is illuminated. The objective of this paper is to model MSA collectors and introduce the necessary quantities that enables MSA collectors to be treated as ordinary flat-plate collectors.

### 2. ATTENUATION OF SOLAR RADIATION IN MSA

When solar radiation enters the MSA slab as shown in Fig. 2, a fraction of the incident energy is transmitted through the material without being attenuated (direct-direct transmittance), a part is removed by scattering and another part is removed by absorption. A portion of the scattered radiation is backscattered and a portion is transmitted through the slab (direct-diffuse transmittance). No correction for surface reflections will be required in the analysis that follows because the index of refraction of MSA is close to unity, between 1.01 and 1.05 depending on density (Henning and Svensson [11]).

The monochromatic direct-direct transmittance is defined by Bouguer's law

$$\tau_{\text{dir-dir},\lambda} = \exp \left[ - \frac{(K_{a,\lambda} + K_{s,\lambda})L}{\cos \theta} \right] \quad (1)$$

The spectral direct-diffuse transmittance,  $\tau_{\text{dir-dif},\lambda}$ , occurs because of scattering within MSA. Analysis of multiple scattering is mathematically complex and requires a great deal of computational effort. However, a new and fast method for isotropic multiple scattering within an absorbing and scattering medium is presented in a latter section.

### 3. OPTICAL TRANSMISSION STUDIES IN MSA

Figure 3 shows measured total (i.e., direct-direct plus direct-diffuse) spectral transmittance in the solar spectrum of a 12 mm thick MSA sample from Tewari *et al.* [23]. A more transparent MSA has been reported by Svendsen [21] who found the total solar transmittance at normal incidence to be 0.9 for a 20 mm thick sample, which is 4% higher than an equally thick sample of Tewari *et al.* However, spectral transmittance values for the Svendsen sample have not yet been reported, so the Tewari data shown in Fig. 3 will be used in this study.

Figure 3 illustrates that the transmittance increases rapidly with wavelength in the visible wavelengths and generally decreases in the near infrared, exhibiting a number of absorption bands. Silica absorbs only slightly in the visible and near ultraviolet, so most of the attenuation of the radiation results from scattering. The absorption bands near 1.4 and 1.9  $\mu\text{m}$  are also seen in water, and the 2.2 and 2.6  $\mu\text{m}$  bands have been identified as combinations of O-H and Si-O fundamentals (Rubin and Lampert [16]).

An isolated spherical particle exhibits Rayleigh scattering if its diameter,  $D$ , is much less than  $\lambda_v/\pi n$ , where  $\lambda_v$  is the vacuum wavelength of incident and scattered light and  $n$  is the index of refraction of the particle. The size of the individual silica particles easily satisfies the criterion for Rayleigh scattering in the visible part of the spectrum (0.4–0.8  $\mu\text{m}$ ). However, MSA is too densely packed to behave as a collection of independent particles, and several authors (Rubin and Lampert [16] and Tewari *et al.* [23]) have attributed

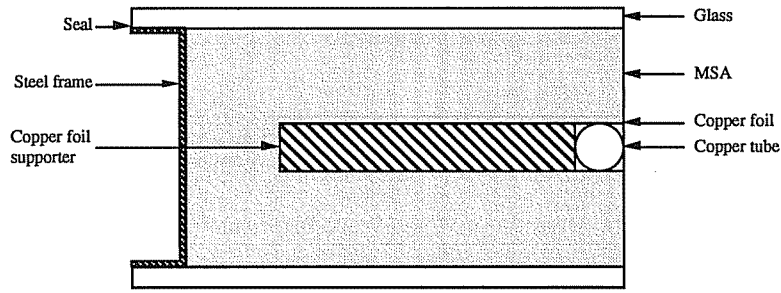


Fig. 1. Cross section of a MSA flat-plate solar collector. Adapted from Svendsen [21].

the primary cause of scattering in MSA to inhomogeneities in the average density such as should be described by dependant scattering theories (e.g., Rayleigh-Debye). Nevertheless, the same authors have assumed independent Rayleigh scattering, and derived a characteristic size for the scatters by fitting the measured transmittance values. In the following the applicability of independent Rayleigh scattering will be tested.

For Rayleigh scattering, the scattered energy in any direction is proportional to the inverse fourth power of the wavelength of the incident radiation. The spectral transmittance for Rayleigh scattering can therefore be written as

$$\tau_{R,\lambda} = \exp\left(-\frac{C}{\lambda^4}\right), \quad (2)$$

where  $\lambda$  is the wavelength of incident and scattered radiation, and  $C$  is an unknown function of the refractive index, the particle size, and volume fraction of MSA. The rising part of the curve in Fig. 3 between 0.3 and 0.8  $\mu\text{m}$  was compared to the inverse fourth-power law of Rayleigh scattering. In Fig. 4 the logarithmic values of the measured transmittance (0.3–0.8  $\mu\text{m}$ ) has been plotted against  $(1/\lambda^4)$ . The agreement between the scattering in MSA and Rayleigh scattering is seen to be very good, and a curve fit of the data to eqn (2) gave a correlation coefficient of 0.999. Thus, even though the particle size distribution is not well

known, it can be assumed that the scattering is Rayleigh.

The optical properties may be found by solving the equation of transfer for Rayleigh scattering. The spectral extinction coefficients are needed as input to this calculation. According to Siegel and Howell [18] the equation of transfer in scattering, absorbing, and emitting media at location  $s$  and direction  $\mu$  can be written as

$$\frac{di_\lambda(s, \mu)}{ds} = -K_{a,\lambda}i_\lambda(s, \mu) + K_{a,\lambda}i_{\lambda b}[T(s), \mu] - K_{s,\lambda}i_\lambda(s, \mu) + \frac{K_{s,\lambda}}{4\pi} \int_{4\pi} i_\lambda(s, \mu) \Phi_\lambda(\omega_i) d\omega_i. \quad (3)$$

The first and third terms on the right-hand side are losses by absorption and scattering, and the second term is the gain by emission. The last term is the gain by scattering from other directions. By introducing the optical thickness,  $\kappa_{D,\lambda} = (K_{a,\lambda} + K_{s,\lambda})s$  and the albedo for scattering,  $\Omega_\lambda = K_{s,\lambda}/(K_{s,\lambda} + K_{a,\lambda})$  and neglecting the emission term, eqn (3) can be written as

$$\frac{di_\lambda(\kappa_{D,\lambda}, \mu)}{d\kappa_{D,\lambda}} = -i_\lambda(\kappa_{D,\lambda}, \mu) + \frac{\Omega_\lambda}{4\pi} \int_{4\pi} i_\lambda(\kappa_{D,\lambda}, \mu) \Phi_\lambda(\omega_i) d\omega_i. \quad (4)$$

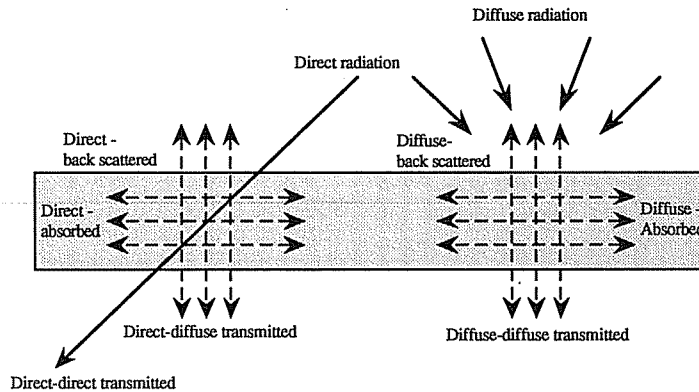


Fig. 2. Distribution of direct, scattered, and adsorbed solar radiation in MSA.

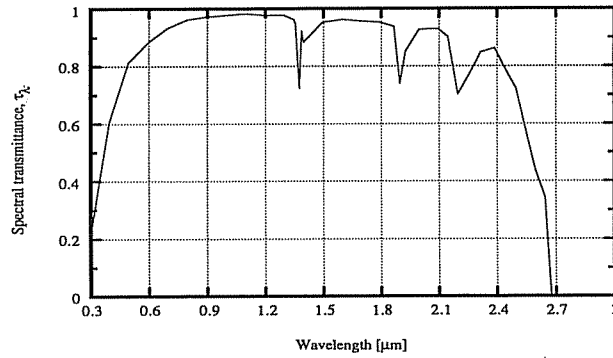


Fig. 3. Total transmission spectrum of 12 mm thick MSA, supercritically dried by CO<sub>2</sub> but not heated to remove all adsorbed H<sub>2</sub>O. Data from Tewari *et al.*[23].

The importance of anisotropy ( $\Phi_{\lambda} \neq 1$ ) has been investigated by several authors (e.g., Evans *et al.*[7]) who calculated the reflectance and transmittance of slabs for different phase functions, albedos, and optical thicknesses. Evans found that the results for isotropic scattering ( $\Phi_{\lambda} = 1$ ) and Rayleigh scattering were nearly identical except at optical thickness exceeding 7 or 8. The MSA optical thickness in the solar spectrum (0.4 to 2.3  $\mu\text{m}$  includes 95% of the terrestrial solar spectrum) is largest in the near ultraviolet region. For a 12 mm thick MSA tile at 0.3  $\mu\text{m}$ , where the albedo for scattering is about 0.8, the optical thickness is  $\sim 1.7$ . Based on Evans' results, the scattering in MSA may be assumed isotropic as long as the tile thickness is less than 50 mm, a thickness that exceeds the probable practical range.

4. RADIATIVE TRANSFER IN AN ABSORBING-SCATTERING MEDIUM

This section presents a new method for predicting the radiative transfer in an absorbing and isotropically scattering plane-parallel atmosphere. The technique is based upon the  $\hat{F}$  ("F-hat") concept (Beckman[2]), and it was developed in order to determine the radiative heat transfer at short wavelengths for MSA.

Consider a one-dimensional plane parallel system of optical thickness  $\kappa_D$  divided into  $n$  equal elements

each of optical thickness  $\Delta\kappa$ , with  $n + 1$  surfaces, as shown in Fig. 5. Solar radiation is incident on surface 1 and short wavelength radiation, that is,  $I$ , is transmitted through the medium while being attenuated by isotropic scattering and absorption along the path. The temperature within the medium is assumed to be low enough to suppress short wavelength emission. Initially the medium will be assumed to be gray.

A factor  $F_{vi,sj}$  is defined as the fraction of the energy isotropically leaving volume element  $i$  that directly impinges on surface  $j$  without being scattered or absorbed along the way.<sup>†</sup> The factors  $F_{vi,sj}$  can be expressed in terms of the third exponential integral,  $E_3(x)$  (see Hottel and Sarofim[9] or Siegel and Howell[18] for definition of the exponential integral).

$$F_{vi,sj} = 2 [|E_3(\kappa_j - \kappa_{i+1}) - E_3(\kappa_j - \kappa_i)|] / 4\Delta\kappa \quad \text{for } j \neq i + 1, i \quad (5)$$

$$F_{vi,sj} = [1 - 2E_3(\Delta\kappa)] / 4\Delta\kappa \quad \text{for } j = i, i + 1. \quad (6)$$

A factor,  $F_{vi,vj}$  is defined as the fraction of energy first scattered in element  $i$  that is attenuated in element  $j$ . The  $F_{vi,vj}$  factors are calculated by

<sup>†</sup> Surface  $j$  can be an "imaginary" surface defining one side of a volume element.

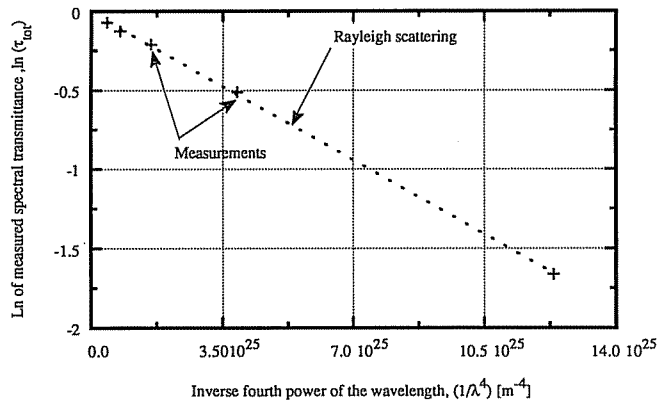


Fig. 4. Comparison of actual scattering in MSA with the  $1/\lambda^4$  variation.

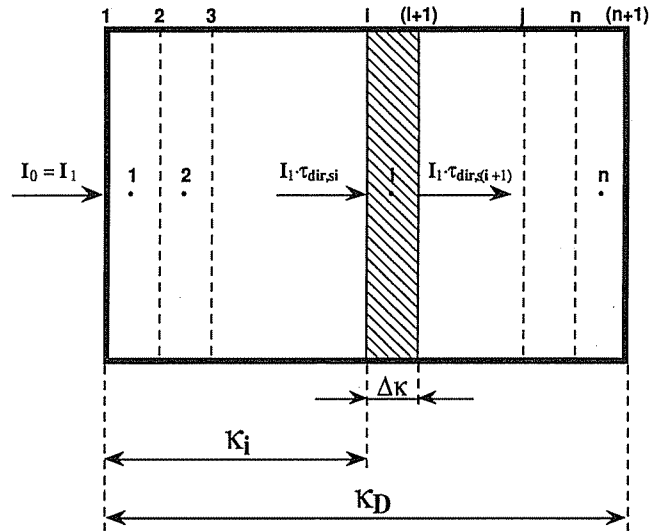


Figure 5. Geometry of plane-parallel system.

$$F_{vi,vj} = |(F_{vi,sj} - F_{vi,s(j-1)})| \quad \text{for } i \neq j \quad (7) \quad I_{att,vk} = I_k - I_{(k+1)}$$

$$F_{vi,vj} = 1 - F_{vi,s(i+1)} - F_{vi,si} \quad \text{for } i = j. \quad (8) \quad = I_1 \cdot [\tau_{dir-dir,sk} - \tau_{dir-dir,s(k+1)}], \quad (12)$$

A related factor  $\hat{F}_{vi,sj}$  is defined as the energy isotropically leaving element  $i$  that strikes surface  $j$  by all possible paths divided by the energy isotropically leaving element  $i$ . The paths include the "direct" component expressed by  $F_{vi,sj}$  as well as all possible paths by which the radiation first scattered in element  $i$  reaches element  $k$ , is scattered in  $k$  and then strikes surface  $j$ . A general expression for  $\hat{F}_{vi,sj}$  for a system divided into  $n$  elements is given by<sup>†</sup>

$$\hat{F}_{vi,sj} = F_{vi,sj} + \sum_{k=1}^n F_{vi,vk} \Omega_k \hat{F}_{vk,sj} \quad (9)$$

$j = 1 \text{ and } n + 1, \quad i = 1 \text{ to } n.$

An expression similar to eqn (9) can be written for every combination of elements and surfaces. The total set of equations for the  $\hat{F}$  factors of  $n$  elements and two surfaces results in  $2n$  sets of  $2n$  linear equations. After evaluating the  $\hat{F}$  factors, the directional reflectance and transmittance of the slab can be calculated by

$$\rho(\theta) = \sum_{k=1}^n \hat{F}_{vk,s1} \Omega_k I_{att,vk} / I_0 \quad (10)$$

$$\tau(\theta) = \tau_{dir-dir} + \sum_{k=1}^n \hat{F}_{vk,s(n+1)} \Omega_k I_{att,vk} / I_0, \quad (11)$$

where  $I_{att,vk}$  is the attenuated energy in element  $k$  and is equal to the decrease in the primary-beam intensity in element  $k$

<sup>†</sup> Only exchange between  $V_i$  and the two real surfaces  $s1$  and  $s(n+1)$  need to be evaluated.

and where  $\tau_{dir-dir,sk}$  is the direct transmittance given by eqn (1), and is a function of the incident angle  $\theta$  of the primary beam. The absorptance of the slab is found from  $\alpha = 1 - \tau - \rho$ .

The number of elements needed to adequately represent the radiative transfer in the one-dimensional plane-parallel slab has been investigated by comparing the transmittance predicted by the  $\hat{F}$ -method with those of the discrete ordinate method, DOM (Siegel and Howell[18]). Two elements are required to obtain a maximum relative error of 1% with respect to the DOM solution for  $\kappa_D$  less than 0.5. At  $\kappa_D$  equal to 1 and 2, the required number of elements have increased to 4 and 10, respectively.

So far only gray media have been considered. However, the extension of the  $\hat{F}$ -method to non-gray media is easy. The monochromatic angular transmittance,  $\tau_\lambda(\theta)$ , and reflectance,  $\rho_\lambda(\theta)$ , values can be calculated in the usual way, with  $\kappa$  replaced by  $\kappa_\lambda$  and  $\Omega$  by  $\Omega_\lambda$ . The total values are then obtained by integration over the solar spectrum (0.3–3  $\mu\text{m}$ ) for each incidence angle.

A major advantage of the  $\hat{F}$ -method compared to techniques such as the DOM or the Zone method (Hottel and Sarofim[9]), is that the  $\hat{F}$ 's are independent of the thermal boundary conditions (assuming that the material properties are independent of changes in the boundary conditions). The importance of this advantage is obvious for angular calculations, where the  $\hat{F}$ 's only need to be evaluated once, even though the source function changes.

## 5. SPECTRAL DEPENDENCE OF TRANSMITTANCE

The measured transmittance values shown in Fig. 3 have been analyzed with the  $\hat{F}$ -method and spectral

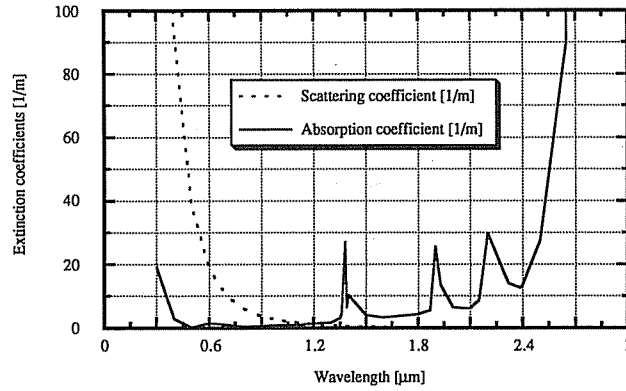


Fig. 6. Spectral scattering and adsorption coefficients for MSA.

absorption and scattering coefficients have been evaluated. The following procedure was applied: Knowing silica hardly absorbs between 0.5 and 0.7 μm (Fricke[8]), the  $\hat{F}$ -method was used to predict the scattering coefficients assuming no absorption occurred in this wavelength interval. An effective size for the scatterers was derived by fitting these scattering coefficients to the following expression for independent Rayleigh scattering

$$K_{s,\lambda} = (1 - \epsilon) \frac{4D_{\text{eff}}^3 \pi^4}{\lambda^4} \left( \frac{n^2 - 1}{n^2 + 2} \right)^2 \quad (13)$$

Multiple scattering in optically thick samples will alter the angular distribution of scattered light. However, if little scattered light re-enters the beam, eqn (13) will still give the correct result for the scattering coefficient. The validity of eqn (13) for MSA was verified in a previous section where the scattering was shown to obey the inverse fourth-power law of independent Rayleigh scattering (see Fig. 4).

The effective particle size derived from curve fitting based on the index of refraction of silica was 7.5 nm. From their micrographs Tewari *et al.*[23] obtained a

mean particle diameter of 4 nm. This discrepancy may be explained by groups of particles behaving as a single scattering unit.

After predicting the effective particle diameter, eqn (13) was used to calculate the spectral scattering coefficients, and combined with the measured transmittance values shown in Fig. 3, the  $\hat{F}$ -method was used to estimate the spectral absorption coefficients. The resulting extinction coefficients are shown in Fig. 6.

Applying the  $\hat{F}$ -method again along with the predicted spectral extinction coefficients, the monochromatic dependence on transmittance, reflectance, and absorption can be studied for different thicknesses and incidence angles. Spectral transmittance and reflectance values for a 20 mm thick MSA tile is shown in Fig. 7 for several incidence angles.

Total values were obtained by integrating the monochromatic values over the entire solar spectrum using the terrestrial distribution given by Wiebelt and Henderson[25]. Calculated values of transmittance, reflectance, and absorptance for a 20 mm thick MSA tile are shown in Fig. 8. The effect of scattering on the transmittance is clearly seen by the increase in total transmittance over the direct-direct transmittance; the

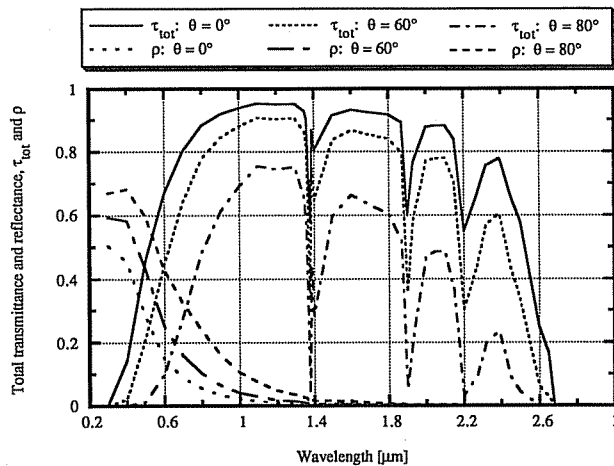


Fig. 7. Calculated spectral transmittance and reflectance at different incidence angles for a 20 mm thick MSA tile.

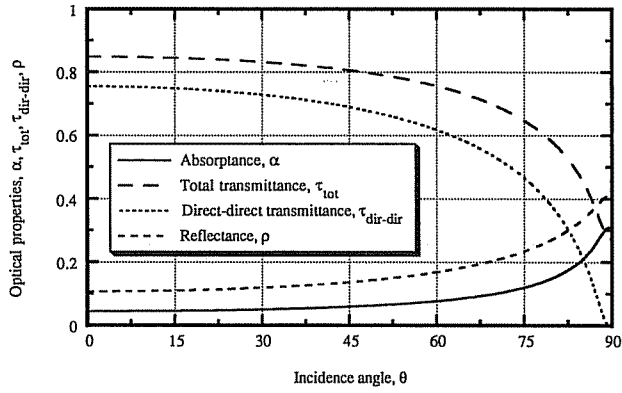


Fig. 8. Calculated transmittance (total and direct-direct), reflectance, and adsorption versus incidence angle for a 20 mm thick MSA tile.

direct-diffuse transmittance is the difference between the total and the direct-direct transmittance curves.

Figure 9 shows the effect of MSA thickness on transmittance. MSA by itself, despite scattering losses in the visible and O-H absorption in the infrared, has a higher total transmittance than conventional glass windows of equal thickness. The total transmittance of a 20 mm-thick MSA tile equals that of single glass. Increasing MSA thickness to 45 mm reduces τ<sub>tot</sub> to about 0.72, equal to double glass.

6. TRANSMITTANCE FOR DIFFUSE RADIATION

The preceding analysis only applied to the beam component of solar radiation. Radiation incident on a collector also consist of scattered solar radiation from the sky and reflected solar radiation from the ground. The transmittance for diffuse radiation, τ<sub>d</sub>, is calculated by

$$\tau_d = \frac{\int_A \tau_b(\theta) \cdot I \cos \theta \, d\omega}{\int_A I \cos \theta \, d\omega}, \quad (14)$$

where A is the range of solid angle of incident diffuse radiation. Brandemuehl and Beckman [3] performed this integration for ordinary glazings by assuming the incident diffuse radiation distribution to be isotropic. The same assumption will be used in this study. Figure 10 shows the effective angle of incident beam radiation, θ<sub>e</sub>, such that τ<sub>d</sub> = τ<sub>b</sub>(θ<sub>e</sub>). The effective incidence angle was found to be independent of thickness at all collector slopes. As shown in the figure, the θ<sub>e</sub> for MSA is lower than for ordinary glazings due to the scattering. The results can be presented as polynomial curve fits as:

$$\theta_e(\text{ground reflected}) = 90.0 - 0.5460\beta + 0.001631\beta^2 \quad (15)$$

$$\theta_e(\text{diffuse sky}) = 55.0 - 0.1913\beta + 0.001984\beta^2. \quad (16)$$

7. INFRARED HEAT TRANSFER IN MSA

The thermal conduction within MSA is composed of two parts. One is a result of solid conduction throughout the aerogel skeleton, and the other is due

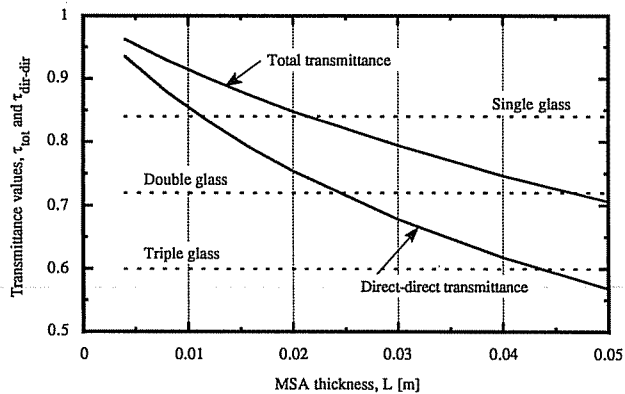


Fig. 9. Calculated total and direct-direct normal-incidence transmittance of MSA versus MSA thickness compared to normal-incidence transmittance of conventional high iron oxide glass windows. All glass is 3 mm clear float glass.

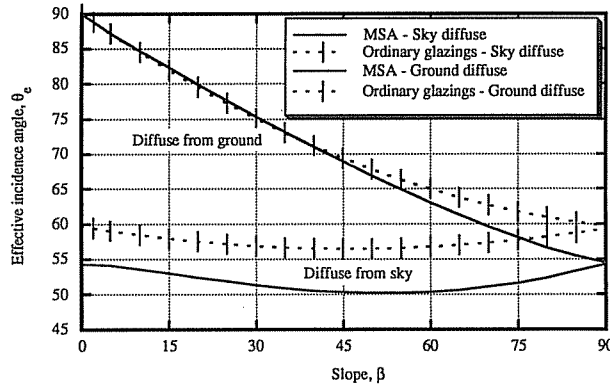


Fig. 10. Effective beam radiation incidence angle for diffuse radiation from sky and ground on tilted MSA tile. The vertical bars indicate the range of results obtained by Brandemuehl and Beckman[3] for ordinary glazings.

to gas conduction within the air pores. The solid conduction is dependent upon MSA density, and the corresponding solid conductivity was found to be about  $0.004 \text{ W/m}^\circ\text{C}$  at a density of  $105 \text{ kg/m}^3$  (Caps and Fricke[4]). The gas conduction varies both with density, temperature, and internal pore pressure,  $p_p$ . As the typical pore size (100 nm) in MSA is smaller than the mean free path of the gas particles, the thermal conductivity of the gas is reduced. In order to eliminate gas conduction the material must be evacuated to a pressure below 20 mbar. The system thus has to be degassed at elevated temperatures and air leakage has to be prevented by use of glass-metal seals (Jensen[10]). For evacuated systems gas conductivity is nearly zero, resulting in a constant conductivity  $\sim 0.004 \text{ W/m}^\circ\text{C}$ . Only evacuated MSA tiles will be considered in this work.

MSA absorbs and emits radiation, but shows no scattering in the infrared because the structural inhomogeneities have dimensions on the order of 100 nm and below, which is much smaller than any infrared wavelength. The spectral absorption coefficient is shown in Fig. 11.

In order to evaluate the insulating properties of MSA it is necessary to consider both infrared radiation

and conduction. Siegel and Howell[18] shows how to integrate eqn (3), over all solid angles and wavelength and equate the results to the net gain by conduction to yield the following nonlinear integro-differential equation for the temperature distribution in the medium

$$k\nabla^2 T - 4 \int_{\lambda=0}^{\infty} K_{a,\lambda} E_{\lambda,b} d\lambda + \int_{\lambda=0}^{\infty} \int_{\omega=0}^{4\pi} K_{a,\lambda} i'_{\lambda}(\omega) d\omega d\lambda = 0. \quad (17)$$

8. COMBINED CONDUCTION AND RADIATION IN AN ABSORBING-EMITTING AND SCATTERING MEDIUM BY THE  $\hat{F}$ -TECHNIQUE

Consider a conducting-radiating medium between two infinite parallel plates spaced a distance  $L$  apart. The plates are gray, isothermal, diffuse reflectors and emitters. Plate 1 is at temperature  $T_1$  and plate 2 is at  $T_2$ . The plate areas are  $A_1$  and  $A_2$ . The homogeneous material between the plates has a constant thermal conductivity, has a refractive index of one, is in local thermodynamic equilibrium and can absorb and emit,

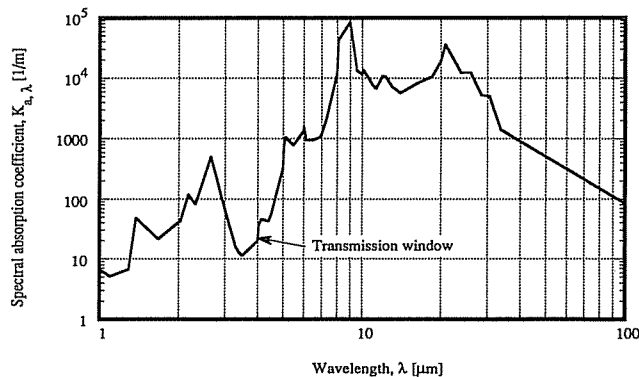


Fig. 11. Absorption coefficient for MSA. Data adapted from Fricke[8].

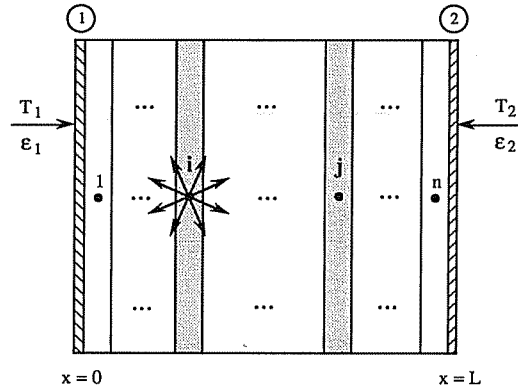


Fig. 12. Schematic diagram of the physical system.

as well as isotropically scatter radiation. Both gray and non-gray media will be considered.<sup>†</sup>

The  $\hat{F}$ -technique begins by subdividing the material into  $n$  volume elements:  $\Delta V_1, \Delta V_2, \dots, \Delta V_n$ , as illustrated by Fig. 12. The method is approximate in the sense that the nonisothermal medium is replaced by a number of finite isothermal subregions. In principle the division can be made as fine as necessary to yield any desired accuracy.

First consider the diffuse radiation leaving surface 1 which impinges on surface 2. Some of the radiation leaving 1 will go directly to 2 and some will reach 2 after one or more reflections and/or scatterings. The total exchange factor between surface 1 and 2,  $\hat{F}_{s1,s2}$ , is defined as the energy isotropically leaving surface 1 that strikes surface 2 by all possible paths divided by the energy isotropically leaving surface 1. Now consider the diffuse radiation leaving surface 1 which is attenuated in volume element  $j$ . Some of the radiation leaving 1 will be directly attenuated in  $j$ , and some will be attenuated in  $j$  after one or more reflections and/or scatterings. The total exchange factor between surface 1 and volume  $j$ ,  $\hat{F}_{s1,vj}$ , is defined as the energy isotropically leaving surface 1 that is attenuated in volume element  $j$  by all possible paths divided by the energy isotropically leaving surface 1. Similar remarks can be made concerning surface 2.

Similarly, some of the radiation leaving volume element  $i$  will go directly to surface 1, and some will reach 1 after one or more reflections and/or scatterings. The total exchange factor between volume element  $i$  and surface 1,  $\hat{F}_{vi,s1}$  is defined as the energy isotropically leaving volume element  $i$  that strikes surface 1 by all possible paths divided by the energy isotropically leaving volume element  $i$ . Finally, some of the diffuse radiation leaving volume element  $i$  which is attenuated in volume element  $j$  will be directly attenuated in  $j$ , and some will be attenuated in  $j$  after one or more reflections and/or scatterings. The total exchange factor between volumes  $i$  and  $j$ ,  $\hat{F}_{vi,vj}$ , is defined as the energy

isotropically leaving volume element  $i$  that is attenuated in volume element  $j$  by all possible paths divided by the energy isotropically leaving volume element  $i$ .

The total exchange factors can be expressed in terms of the direct exchange factors,  $F_s$ , diffuse reflectances,  $\rho_s$ , albedos for scattering,  $\Omega_s$ , and other  $\hat{F}$ 's in the following manner

$$\hat{F}_{s1,sj} = F_{s1,sj} + \sum_{k=1}^2 F_{s1,sk} \rho_k \hat{F}_{sk,sj} + \sum_{k=1}^n F_{s1,uk} \Omega_k \hat{F}_{uk,sj} \quad i = 1, 2 \quad \text{and} \quad j = 1, 2 \quad (18)$$

$$\hat{F}_{s1,vj} = F_{s1,vj} + \sum_{k=1}^2 F_{s1,sk} \rho_k \hat{F}_{sk,vj} + \sum_{k=1}^n F_{s1,uk} \Omega_k \hat{F}_{uk,vj} \quad i = 1, 2 \quad \text{and} \quad j = 1 \text{ to } n \quad (19)$$

$$\hat{F}_{vi,sj} = F_{vi,sj} + \sum_{k=1}^2 F_{vi,sk} \rho_k \hat{F}_{sk,sj} + \sum_{k=1}^n F_{vi,uk} \Omega_k \hat{F}_{uk,sj} \quad i = 1 \text{ to } n \quad \text{and} \quad j = 1, 2 \quad (20)$$

$$\hat{F}_{vi,vj} = F_{vi,vj} + \sum_{k=1}^2 F_{vi,sk} \rho_k \hat{F}_{sk,vj} + \sum_{k=1}^n F_{vi,uk} \Omega_k \hat{F}_{uk,vj} \quad i = 1 \text{ to } n \quad \text{and} \quad j = 1 \text{ to } n. \quad (21)$$

The values of the direct exchange factors can be expressed in terms of the third exponential integral as given by eqns (5) and (6). It is also worth mentioning that eqns (9) and (20) are identical except for the third term in eqn (20) which accounts for reflections from the boundary plates. This term is ignored in eqn (9) due to the fact that the surface reflections in MSA can be neglected and that no boundary plates are present in the system modeled in Fig. 5.

Equations (18) to (21) must be solved simultaneously. Relationships between the  $\hat{F}$ 's can reduce the computational effort. These properties are the summation rule and the reciprocity rule and are similar to the summation and reciprocity rules for view factors. The summation rule can be developed by recognizing that the energy leaving a surface or a volume element must ultimately be absorbed by the surface and the volume elements in the system. The energy originating from surface or volume  $i$  that is absorbed by surface  $j$  is  $\epsilon_j \hat{F}_{ij}$ , where the absorptance  $\alpha_j$  has been replaced by the emittance  $\epsilon_j$  since the surfaces are gray (or the analysis is monochromatic). Similarly,  $(1 - \Omega_j) \hat{F}_{ij}$  denotes the energy absorbed by volume element  $j$  from either surface or volume  $i$ . Since all the energy must be absorbed, the sum over all surfaces and volume elements must be equal to unity.

$$\sum_{k=1}^2 \epsilon_k \hat{F}_{si,sk} + \sum_{k=1}^n (1 - \Omega_k) \hat{F}_{si,vk} = 1 \quad i = 1, 2 \quad (22)$$

$$\sum_{k=1}^2 \epsilon_k \hat{F}_{vi,sk} + \sum_{k=1}^n (1 - \Omega_k) \hat{F}_{vi,vk} = 1$$

$$\text{for } i = 1 \text{ to } n. \quad (23)$$

<sup>†</sup> A subscript to separate monochromatic and gray values will not be used. Whenever the meaning is not clear,  $\lambda$  will be introduced to denote monochromatic values.

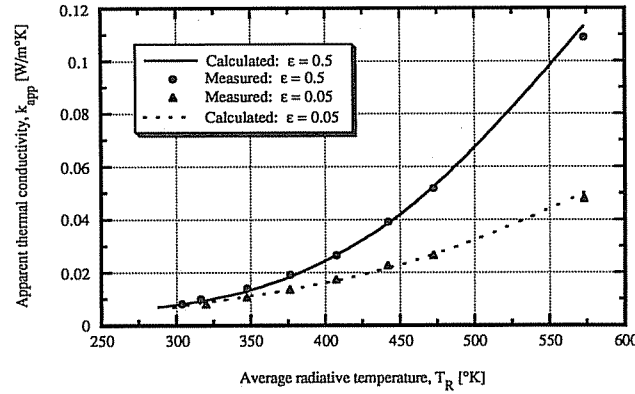


Fig. 13. Apparent thermal conductivity of MSA under variation of average radiative temperature. Comparison of the  $\hat{F}$ -method and measurements at two different boundary emissivities.

It can be shown that the total exchange factors obey the laws of reciprocity:

$$A_j \hat{F}_{sj,si} = A_i \hat{F}_{si,sj} \quad \text{for } i \text{ and } j = 1, 2 \quad (24)$$

$$A_i \hat{F}_{si,vj} = 4K_{T,j} \Delta V_j \hat{F}_{vj,si} \quad \text{for } i = 1, 2 \text{ and } j = 1 \text{ to } n \quad (25)$$

$$\Delta V_i \hat{F}_{vi,vj} = \Delta V_j \hat{F}_{vj,vi} \quad \text{for } i \text{ and } j = 1 \text{ to } n. \quad (26)$$

By means of the total exchange factors, the inner integral in the absorption term in eqn (17) can be replaced by summation terms and an energy balance can be written for each volume element. For a non-gray medium the energy balance for volume element  $i$  is<sup>||</sup>

$$\begin{aligned} k \nabla^2 T_{vi} \Delta V_i - 4 \Delta V_i \sigma T_{vi}^4 \int_{\lambda=0}^{\infty} K_{ai,\lambda} f_{\lambda T} d\lambda \\ + \sum_{k=1}^2 \epsilon_k A_k \sigma T_{sk}^4 \int_{\lambda=0}^{\infty} \hat{F}_{(sk,vi),\lambda} (1 - \Omega_{i,\lambda}) d\lambda \\ + \sum_{k=1}^n 4 \Delta V_k \sigma T_{vk}^4 \int_{\lambda=0}^{\infty} K_{ak,\lambda} f_{\lambda T} \hat{F}_{(vk,vi),\lambda} \\ \times (1 - \Omega_{i,\lambda}) d\lambda = 0, \quad (27) \end{aligned}$$

with

$$f_{\lambda T} = \frac{C_1}{\sigma T^4 \lambda^5 \left[ \exp\left(\frac{C_2}{\lambda T}\right) - 1 \right]}. \quad (28)$$

The first term in eqn (27) is the conduction contribution to volume element  $i$ , the second term is the energy emitted from volume element  $i$ , and the third and fourth terms represent the energy absorbed in volume element  $i$ , being originally emitted from the sur-

faces and volume elements in the enclosure, respectively.

The temperature distribution within the medium was found by expressing the conduction term in finite-difference form, and solving the  $n$  nonlinear equations by Newton-Raphson techniques. Once the temperature distribution has been evaluated, the final step in the solution procedure is to calculate the heat transfer across the medium from plate 1 to plate 2. The total heat flux,  $q_{tot}$ , at surface  $x = 0$  can be expressed by the conduction term at surface 1 plus the difference between the radiation emitted by surface 1 and the radiation absorbed by surface 1. For a non-gray medium

$$\begin{aligned} q_{tot} = - \left( k \frac{dT}{dx} \right)_{x=0} + \epsilon_1 A_1 \sigma T_{s1}^4 - \epsilon_1 \sum_{k=1}^2 \epsilon_k A_k \sigma T_{sk}^4 \\ \times \int_{\lambda=0}^{\infty} \hat{F}_{(sk,s1),\lambda} d\lambda - 4 \epsilon_1 \sum_{k=1}^n \Delta V_k \sigma T_{vk} \\ \times \int_{\lambda=0}^{\infty} K_{ak,\lambda} f_{\lambda T} \hat{F}_{(vk,s1),\lambda} d\lambda. \quad (29) \end{aligned}$$

Comparison of results for the gray case is made with the results of Viskanta [24]. Viskanta's results can be exactly reproduced by the  $\hat{F}$ -method as long as the grid spacing is made fine enough. The radiative flux reached Viskanta's solution within 1% in all cases with a uniform subdivision of 30. However, the conductive term required a subdivision of five times as fine to obtain the same accuracy, and the computer time was unacceptably high. The necessity for fine grid spacing is due to the calculation of the temperature gradient at  $x = 0$ . To overcome this obstacle and use computer power more effectively, nonuniform grid spacing was introduced near plate 1. A very fine subdivision was employed to the four volume elements closest to plate 1, and a more coarse and uniform division was used for the rest of the geometry. In this way the number of grids necessary to obtain an accurate solution was reduced from 150 to 30 for a typical calculation.

As the absorption coefficient in MSA is strongly wavelength dependent, eqn (28) with  $\Omega = 0$  was em-

<sup>||</sup> The gray form of eqn (27) is obtained by replacing the integrals by the average value of the integrands.

ployed to calculate the temperature distribution within the medium. The calculated heat flux for a 20 mm thick and evacuated MSA tile is compared to experimental data published by Scheuerpflug *et al.*[17] in Fig. 13. The comparison was done in terms of the so called apparent thermal conductivity,  $k_{app}$ , as a function of the medium average radiative temperature,  $T_R$  for two values of the boundary surface emittances, 0.05 and 0.50. The predictions obtained with the  $\bar{F}$ -method agree very well with the measurements, and the agreement is much better than the simplified procedure proposed by Caps and Fricke[4].

#### 9. TRANSMITTANCE-ABSORPTANCE PRODUCT FOR MSA COLLECTORS

Since MSA requires protection against the elements, glass must be used as the outside cover. For clear angle-preserving covers such as glass panes or honeycombs,  $(\tau\alpha)$ -products have been evaluated by several authors (e.g., Edwards[6] and Symons[22]), but the inclusion of scattering layers or irregularly reflecting layers complicates the calculation. In the following section an approximate method which allows the inclusion of scattering layers is derived based on the embedding technique presented by Edwards[6].

To employ the embedding technique one imagines a stack of  $n$  elements including an absorber plate and  $n - 1$  covers, and one formulates the effect of adding one more element to the array. The assumptions are restrictive, but allow the inclusion of scattering layers with sufficient accuracy for most cases. The diffuse reflections from the absorber will be assumed to be isotropic. Transmitted or reflected fluxes from a single layer will be split up into components: A direct, angle-preserving component for the incidence angle under consideration, and a component deflected by scattering or reflection, which will be treated as isotropic. Figure 14 shows the angular distribution of the backscattered (reflected) radiation from a slab with isotropic scattering, and it is obvious that the distribution is not isotropic.

In order to assess the errors introduced by assuming an isotropic distribution, three different values of the

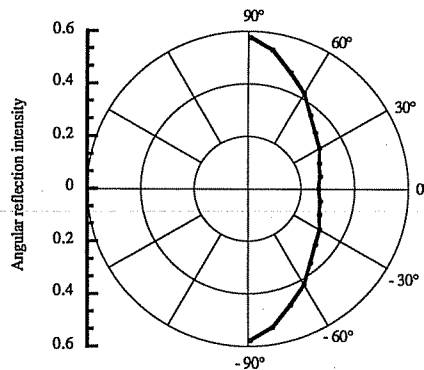


Fig. 14. Angular distribution of diffuse reflections from a plane-parallel atmosphere with isotropic scattering of finite optical thickness and an albedo of 0.9.

integrated reflectance and transmittance were employed: (a) values based on the largest angular intensity; (b) values based on the smallest angular intensity; and (c) values based on the integrated intensities. In all cases an isotropic distribution was assumed. The analysis showed that the difference in estimating the  $(\tau\alpha)$ -product for the MSA collector in Fig. 1 was less than 4% for the different approaches with approach (c) being between (a) and (b). The authors feel that the proposed method which is based on (c) is acceptable. Calculations have shown that this approximation may be used even for extremely anisotropic distributions if the actual is replaced by an effective isotropic distribution (McKellar and Box[15]).

The transmittance of the  $i$ th cover is therefore divided into a direct-direct (i.e., beam) component,  $\tau_i^b$ , and a direct-diffuse (i.e., scattered) component,  $\tau_i^s$ . Similarly, the reflectances of the  $i$ th cover are denoted by  $\rho_i^b$  and  $\rho_i^s$ , respectively, for the inside surface and  $\rho_i^b$  and  $\rho_i^s$  for the outside surface of the element. The transmittance of any element is the same from either direction due to the reciprocity principle. The absorptances of element  $i$  for beam radiation from each direction,  $\alpha'_i$  and  $\alpha_i$  are given by

$$\alpha'_i = 1 - \rho_i^{b'} - \rho_i^{s'} - \tau_i^b - \tau_i^s \quad (30)$$

$$\alpha_i = 1 - \rho_i^b - \rho_i^s - \tau_i^b - \tau_i^s. \quad (31)$$

The transmittance and reflectances for diffuse fluxes incident on the  $i$ th element are denoted by  $\tau_i^d$ ,  $\rho_i^d$ , and  $\rho_i^{d'}$ . The diffuse absorptances of element  $i$  can then be expressed as

$$\alpha_i^{d'} = 1 - \rho_i^{d'} - \tau_i^d \quad (32)$$

$$\alpha_i^d = 1 - \rho_i^d - \tau_i^d. \quad (33)$$

Allowance is thus made for optical coatings such as antireflection films and/or thin oxide IR-reflecting films being different on each face of each coverglass element.

The incident flux from outside the system,  $q_{n+1}^-$ , is direct and normalized to unity. The leaving fluxes are made up of a direct and a diffuse component,  $q_{n+1}^{+b}$  and  $q_{n+1}^{+d}$ , respectively, as illustrated in Fig. 15. Since  $q_{n+1}^-$  is normalized to unity, the outgoing fluxes are given by the following relationships

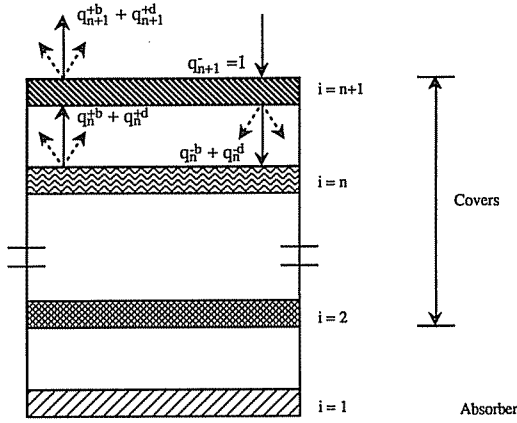
$$q_{n+1}^{+b} = R_{n+1}^b \quad (34)$$

$$q_{n+1}^{+d} = R_{n+1}^s, \quad (35)$$

where  $R_{n+1}^b$  and  $R_{n+1}^s$  are the top-of-the- $n + 1$ -stack reflectances due to the reflection of the direct incident flux and scattering, respectively. The incoming fluxes for the  $n$ th cover element are

$$q_n^{-b} = \tau_{n+1}^b + \rho_{n+1}^{b'} \cdot q_n^{+b} \quad (36)$$

$$q_n^{-d} = \tau_{n+1}^d + \rho_{n+1}^{d'} \cdot q_n^{+d} + \rho_{n+1}^{s'} \cdot q_n^{+b}. \quad (37)$$

Fig. 15. Embedding a stack of  $n$  covers.

Similarly, the outgoing fluxes can be expressed by the following expressions

$$q_n^{+b} = R_n^b \cdot q_n^{-b} \quad (38)$$

$$q_n^{+d} = R_n^s \cdot q_n^{-b} + R_n^d \cdot q_n^{-d}, \quad (39)$$

where  $R_n^d$  is the top-of-the- $n$ -stack reflectance due to reflections of diffuse fluxes. Combining eqns (36) and (38) and eqns (37) and (39) yields

$$q_n^{-b} = \frac{\tau_{n+1}^b}{(1 - \rho_{n+1}^b \cdot R_n^b)} \quad (40)$$

$$q_n^{-d} = \frac{\tau_{n+1}^s}{(1 - \rho_{n+1}^d \cdot R_n^d)} + q_n^{-b} \times \left[ \frac{\rho_{n+1}^{s} \cdot R_n^b + \rho_{n+1}^{d} \cdot R_n^s}{(1 - \rho_{n+1}^d \cdot R_n^d)} \right]. \quad (41)$$

For convenience, top-of-the-stack transmittances are defined. For the incident beam radiation

$$t_{n+1}^b = \frac{q_n^{-b}}{q_{n+1}^{-b}} = q_n^{-b}, \quad (42a)$$

for the incident beam radiation that is scattered

$$t_{n+1}^s = \frac{q_n^{-d}}{q_{n+1}^{-b}} = q_n^{-d}, \quad (42b)$$

and for the incident diffuse radiation (used latter)

$$t_{n+1}^d = \frac{\tau_{n+1}^d}{(1 - \rho_{n+1}^d \cdot R_n^d)}. \quad (42c)$$

The outgoing fluxes above the new element are

$$q_{n+1}^{+b} = \rho_{n+1}^b + \tau_{n+1}^b \cdot q_n^{+b} \quad (43)$$

$$q_{n+1}^{+d} = \rho_{n+1}^s + \tau_{n+1}^s \cdot q_n^{+b} + \tau_{n+1}^d \cdot q_n^{+d}. \quad (44)$$

Substituting eqns (34) and (38) into eqn (43), and

eqns (35) and (39) into eqn (44), along with the definitions given by eqns (42a) and (42b), yield the desired relations for the overall reflectances of the stack embedded by one more cover for incident beam radiation

$$R_{n+1}^b = \rho_{n+1}^b + \tau_{n+1}^b \cdot R_n^b \cdot t_{n+1}^b \quad (45)$$

$$R_{n+1}^s = \rho_{n+1}^s + \tau_{n+1}^s \cdot R_n^b \cdot t_{n+1}^b + \tau_{n+1}^d \cdot [R_n^s \cdot t_{n+1}^b + R_n^d \cdot t_{n+1}^s]. \quad (46)$$

In a similar manner (with the definition of diffuse transmittance given by eqn (42c)) the overall reflectance of the stack embedded by one more cover for incident diffuse radiation is

$$R_{n+1}^d = \rho_{n+1}^d + \tau_{n+1}^d \cdot R_n^d \cdot t_{n+1}^d. \quad (47)$$

A top-of-the-stack absorptance is introduced as

$$a_{n+1} = \alpha'_{n+1} \cdot q_n^{+b} + \alpha_{n+1} \cdot q_n^{-b} + \alpha'^d_{n+1} \cdot q_n^{+d} + \alpha_{n+1} \cdot q_n^{-d}. \quad (48)$$

From eqns (38) to (47), eqn (48) can be rewritten as

$$a_{n+1} = \alpha'_{n+1} \cdot R_n^b \cdot t_{n+1}^b + \alpha_{n+1} + \alpha'^d_{n+1} \times (t_{n+1}^b \cdot R_n^s + t_{n+1}^s \cdot R_n^d). \quad (49)$$

For an  $N$ -element stack subjected to normalized solar radiation, one can find the fraction  $A_{N,N}$  of the radiation absorbed by the outermost cover from the value  $a_N$ . For each successive element below the outer one the downgoing flux is

$$q_i^{-(b+d)} = t_{i+1}^b \cdot q_{i+1}^{-b} + t_{i+1}^s \cdot q_{i+1}^{-b} + t_{i+1}^d \cdot q_{i+1}^{-d}, \quad (50)$$

beginning with  $i = N$ . The within-stack absorptance  $A_{i,N}$  is then given by the following relation

$$A_{i,N} = a_i \cdot t_{i+1}^b \cdot q_{i+1}^{-b} + a_i^d \times [t_{i+1}^s \cdot q_{i+1}^{-b} + t_{i+1}^d \cdot q_{i+1}^{-d}]. \quad (51)$$

Conservation of energy can be used to check the calculations.

$$R_N^b + R_N^s + A_{1,N} + A_{2,N} + \dots + A_{N,N} = 1. \quad (52)$$

The procedure for calculating the  $(\tau\alpha)$ -product starts with calculating the single layer transmittances and reflectances. The embedding calculation then starts with the bare absorber

$$R_1^b = [1 - \alpha(\theta)] \cdot \left(1 - \frac{\rho_{\text{dif}}}{\rho_{\text{tot}}}\right), \quad (53)$$

$$R_1^s = [1 - \alpha(\theta)] \cdot \frac{\rho_{\text{dif}}}{\rho_{\text{tot}}}, \quad (54)$$

$$a_1 = \alpha_{\text{abs}}(\theta). \quad (55)$$

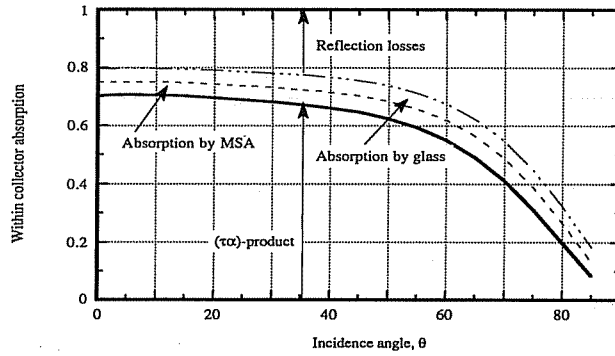


Fig. 16. Within-stack absorption versus incidence angle for the MSA collector.

Then the first cover, element 2, is added, and  $t_2^b$ ,  $t_2^s$ ,  $R_2^b$ ,  $R_2^s$ , and  $a_2$  are found from the above equations. Then the second cover is added and so on until the outermost  $N$ th element is included.<sup>§</sup>

By repeated use of eqns (50) and (51) the solar absorptance by each element within the collector can be evaluated. Figure 16 shows the within-stack absorptions versus incidence angle for the MSA collector. At normal incidence 72% of the solar radiation is absorbed by the absorber plate, 3.8% is absorbed by the MSA tile, 4.2% is absorbed by the glass cover and 20% is reflected away.

#### 10. INCIDENCE ANGLE MODIFIER FOR MSA COLLECTORS

The  $(\tau\alpha)$ -product is dependent on the collector configuration and varies with the angle of incidence as well as with the relative values of diffuse and beam radiation. To model this dependence an incidence angle modifier can be introduced into the Hottel-Whillier collector model. Souka and Safwat [19] suggested that the incidence angle modifier can be written

$$K_{\tau\alpha} = \frac{(\tau\alpha)}{(\tau\alpha)_n} \quad (56)$$

Standard test methods [ASHRAE [1]] include experimental estimation of this effect by assuming the entire radiation to be beam, and to use the following expression for the angular dependence of  $K_{\tau\alpha}$

$$K_{\tau\alpha} = 1 + b_0 \left( \frac{1}{\cos \theta} - 1 \right), \quad (57)$$

where  $b_0$  is the incidence angle modifier coefficient. The calculated incidence angle modifier is shown in Fig. 17 for the MSA collector as a function of  $[(1/\cos \theta) - 1]$ . It is seen that  $K_{\tau\alpha}$  is linear all the way out to values of the abscissa of 2, corresponding to an incidence angle of  $75^\circ$ . The value of  $b_0$  was determined to  $-0.22$ .<sup>#</sup>

Equation 57 presumes that all incident radiation strikes the collector at the same incidence angle, which is not true because of the presence of diffuse and ground-reflected radiation. By assuming isotropic dif-

<sup>§</sup> For an architectural application, the effective reflectance of the room behind the window is used for  $R_1$ .

<sup>#</sup> Equation (57) gives misleading results for ordinary glazings at incidence angles larger than  $60^\circ$ .

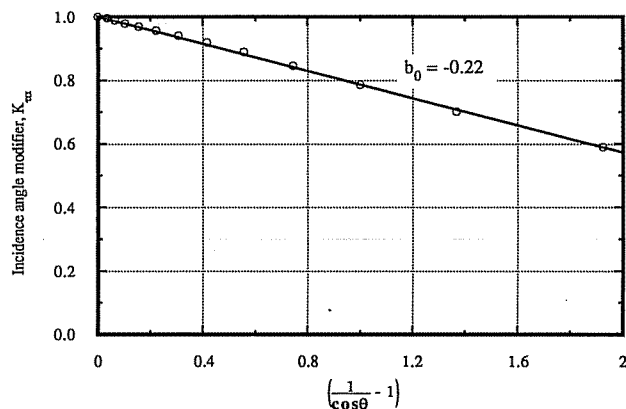


Fig. 17. Incidence angle modifier coefficient as a function of  $(1/\cos \theta) - 1$ .

fuse radiation, the absorbed solar radiation,  $S$ , can be expressed as

$$S = (\tau\alpha)_n \left[ I_b R_b K_{\tau\alpha,b} + I_d \frac{(1 + \cos \beta)}{2} K_{\tau\alpha,d} + \rho_g I \frac{(1 - \cos \beta)}{2} K_{\tau\alpha,g} \right]. \quad (58)$$

The subscripts b, d, and g represent beam, diffuse, and ground-reflected. For a given collector tilt, the same procedure as described earlier was used to calculate effective beam incidence angles for the  $(\tau\alpha)$ -product of diffuse sky and ground reflected radiation. The input to this calculation was the incidence angle dependent  $(\tau\alpha)$ -product predicted by the modified embedding technique. This analysis revealed that the effective incidence angles evaluated for the transmittance in MSA was also valid for the  $(\tau\alpha)$ -product in MSA collectors. Equation (58) can be written in terms of a total incidence angle modifier as follows

$$S = I_T K_{\tau\alpha} (\tau\alpha)_n, \quad (59)$$

where the total incidence angle modifier is given by

$$K_{\tau\alpha} = \frac{I_b}{I_T} R_b \left[ 1 + b_0 \left( \frac{1}{\cos \theta} - 1 \right) \right] + \frac{I_d}{I_T} \left( \frac{1 + \cos \theta}{2} \right) \times \left[ 1 + b_0 \left( \frac{1}{\cos \theta_{e,d}} - 1 \right) \right] + \rho_g \frac{I}{I_T} \left\{ \left( \frac{1 - \cos \beta}{2} \right) \times \left[ 1 + b_0 \left( \frac{1}{\cos \theta_{e,g}} - 1 \right) \right] \right\}. \quad (60)$$

## 11. COLLECTOR OVERALL HEAT LOSS COEFFICIENT

In order to use the Hottel-Whillier collector equation an overall heat loss coefficient,  $U_L$ , must be evaluated for the MSA collector. A general energy analysis includes solar radiation, long-wavelength radiation, conduction and convection due to wind. Except for the wind effects, all of these mechanisms have been

discussed. The cover system was divided into appropriate nodes, and energy balance equations were written for each. Based on these calculated temperatures an apparent thermal conductivity was evaluated for the MSA tile. The top loss coefficient,  $U_t$ , was evaluated for different absorber plate temperatures, absorber plate emittances, wind heat transfer coefficients, and ambient and sky temperatures.

The use of a blackbody radiation sky temperature not equal to the air temperature did not significantly effect  $U_t$ . Less than 1% increase in  $U_t$  was observed when the sky temperature was reduced from 10 to 0°C. The same percentage change (decrease) was found at an absorber plate temperature of 150°C when the absorber plate emittance was changed from 0.9 to 0.1. The negligible loss reduction obtained by selective coatings was expected due to the low apparent thermal conductivity in MSA. An increase in  $U_t$  on the order of 1% was observed when the wind heat transfer coefficient was increased from 5 to 20 W/m<sup>2</sup> K. This change is much smaller than for ordinary collectors, and is also explained by the insulation properties of MSA.

When a similar analysis is performed for collectors with ordinary glazings, it is assumed that the absorbed solar radiation by covers will not affect the losses from the collector. This effect is accounted for by introducing an effective transmittance-absorptance product (Duffie and Beckman [5]). Even through the term concerning absorbed solar radiation can be included in the analysis, it will be ignored in the following calculations. By doing this, and evaluating an effective transmittance-absorptance product for the MSA collector, the simplicity of the theory for ordinary flat-plate collectors is maintained.

The calculation of the top loss coefficient for the MSA collector is a very tedious process. The simplify the evaluation of collector performance, Fig. 18 has been prepared. The figure shows the top loss coefficient for the MSA collector in Fig. 1 for: ambient temperatures of 25, 10, and -10°C for a range of absorber plate temperatures. The effect of MSA thickness is also included in the figure. In this case the ambient tem-

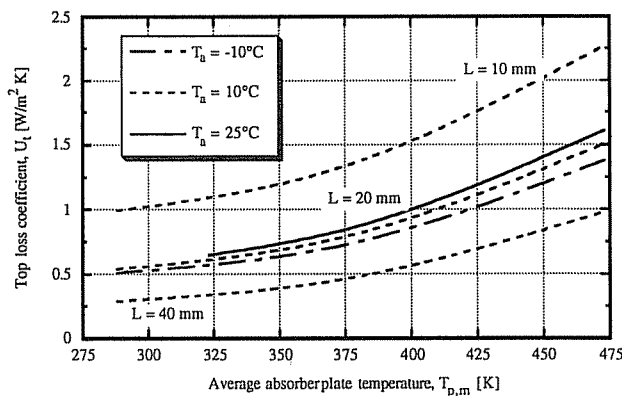


Fig. 18. Top loss coefficient versus average absorber plate temperatures at different ambient temperatures.

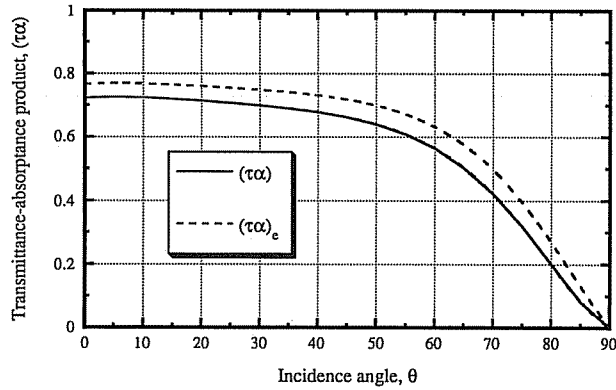


Fig. 19.  $(\tau\alpha)$  and  $(\tau\alpha)_e$  versus incidence angle.

perature was kept at 10°C. The calculations were performed using a wind heat transfer coefficient of 10 W/m<sup>2</sup> °C.

The figure shows that  $U_i$  is strongly dependent upon the absorber plate temperature and the MSA thickness. The ambient temperature is also seen to play an important role, while the other parameters have minor influence on  $U_i$ . To use Fig. 18, it is necessary to know the mean absorber plate temperature,  $T_{p,m}$ . Duffie and Beckman [5] present a method for estimating  $T_{p,m}$  and also present information on how to estimate the back and edge losses that must be added to  $U_i$ , to determine  $U_L$ . Once  $U_L$  is known,  $F_R$ , the collector heat removal factor, can be found by standard methods.

## 12. EFFECTIVE TRANSMITTANCE-ABSORPTANCE PRODUCT

To maintain the simplicity of Hottel-Whillier collector equation, and account for the reduced losses due to absorption of solar radiation by the covers, Duffie and Beckman introduced an effective transmittance-absorption product,  $(\tau\alpha)_e$ . The same approach was followed for the MSA collector. Figure 19 illustrates the difference between  $(\tau\alpha)_e$  and  $(\tau\alpha)$  versus incidence angle. The incident angle modifier,  $b_0$ , for  $(\tau\alpha)_e$  is

found from Fig. 19 to be  $-0.18$ , somewhat less than the  $-0.22$  found for  $(\tau\alpha)$ .

## 13. MSA COLLECTOR PERFORMANCE

The Hottel-Whillier equation can be written in terms of an "instantaneous" efficiency as

$$\eta_i = \frac{Q_u}{A_c G_T} = F_R K_{\tau\alpha} (\tau\alpha)_e - F_R U_L \frac{(T_i - T_a)}{G_T} \quad (61)$$

The efficiency of the MSA collector shown in Fig. 1 has been measured at the Thermal Insulation Laboratory in Denmark (Svendsen [21]). The calculation procedure developed in this paper has been compared with the Danish measurements under similar conditions. As shown in Fig. 20 there is good agreement between the calculated and measured efficiency.

The model underpredicts the measured heat loss coefficient by about 10%. This was expected due to the deviations from the ideal preconditioning of MSA used in the collector as stated by Svendsen [21]. The predicted optical efficiency is also lower than the measurements. This is related to the spectral extinction data used as input to the model. Due to lack of spectral

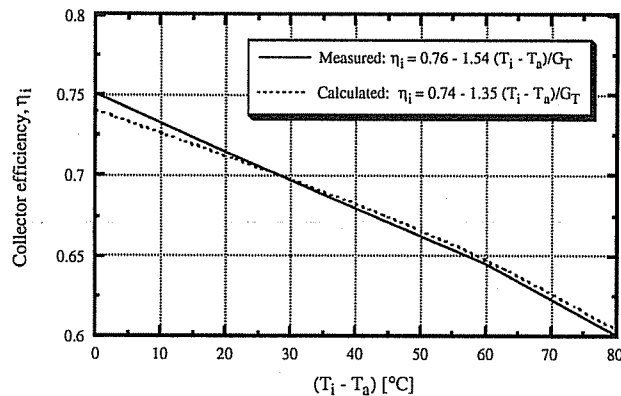


Fig. 20. Comparison of calculated and measured efficiency curves at  $G_T = 800$  W/m<sup>2</sup>.

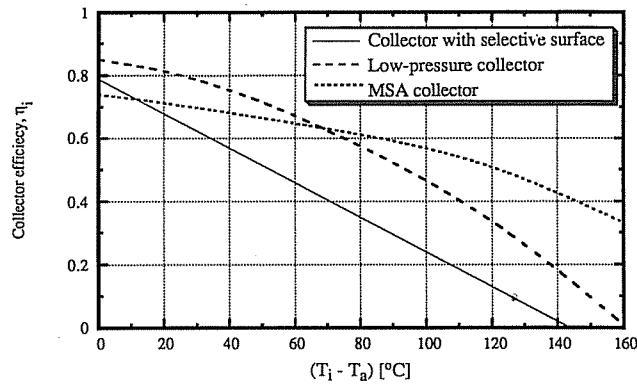


Fig. 21. Collector efficiency as a function of the difference between fluid inlet and ambient temperatures.

measurements of the MSA used in the Danish collector, these data had to be developed from another type of MSA, which is about 4% less transparent.

#### 14. COMPARISON OF MSA COLLECTORS WITH OTHER COLLECTOR DESIGNS

Instantaneous collector efficiencies are shown in Fig. 21 for three different collector designs: (a) one cover with selective absorber plate ( $\epsilon_p = 0.065$ ); (b) low-pressure flat-plate collector (from Kellner [14]); and (c) MSA collector. The incident radiation on the collectors was  $800 \text{ W/m}^2$ .

It is clearly seen that considerable improvements of the efficiency can be obtained by using MSA collectors for high temperature applications. The efficiency is even better than the low-pressure flat-plate collector for temperature differences larger than about  $65^\circ\text{C}$ .

#### 15. ANNUAL PERFORMANCE

A single glazed flat-plate collector with selective coating characterized by  $F_R(\tau\alpha) = 0.80$  and  $F_R U_L = 4.20 \text{ W/m}^2\text{C}$  is used as a reference. Table 1 indicates possible improvements to this reference collector. The annual performances estimates were obtained with TRNSYS for a process heating application in Madison, WI, at a minimum operating temperature of  $75^\circ\text{C}$ . The MSA collector clearly outperforms the other for this application.

In Sweden large selective surface flat-plate collector areas are used in district heating networks. These col-

lectors are required to operate at temperatures between  $60$  and  $100^\circ\text{C}$ . Collectors with a single teflon film plus selective coatings have been proposed to replace the existing collectors (Karlsson [12,13]). The corrugated teflon film collector and the honeycomb collector can be expected to increase the annual gain by 7 and 11%, respectively, but will not be used because of their high cost. The MSA collector can increase the yearly gain by as much as 41%. Today, MSA collectors are not commercially available and are far too expensive. However, when MSA is mass produced and the MSA collector is fully developed it is expected that the collector will be a significant breakthrough for solar heating systems at medium and high temperatures.

#### NOMENCLATURE

- $A_k$  area of surface  $k$  ( $\text{m}^2$ )
- $C_1$  Planck's first radiation constant ( $3.7405 \cdot 10^{-16} \text{ W m}^2$ )
- $C_2$  Planck's second radiation constant ( $0.0143879 \text{ W K}$ )
- $f_{\lambda T}$  weight function of Planck's spectral distribution of emissive power
- $\bar{F}_{vk,vi}$  total exchange factor between volume element  $k$  and volume element  $i$
- $\bar{F}_{sk,vi}$  total exchange factor between surface  $k$  and volume element  $i$
- $I$  solar radiation intensity
- $i_a$  directional monochromatic radiation intensity
- $i_{\lambda b}$  monochromatic intensity of emitted energy of the particles
- $k$  thermal conductivity ( $\text{W/m K}$ )
- $k_{\text{app}}$  apparent thermal conductivity,  $q_{\text{tot}} L / (T_1 - T_2)$  ( $\text{W/m K}$ )
- $K_{ak}$  absorption coefficient in volume  $k$  ( $1/\text{m}$ )
- $K_{a,\lambda}$  absorption coefficient ( $1/\text{m}$ )

Table 1. Simulated yearly heat production at a minimum operating temperature of  $75^\circ\text{C}$

Collector type	$F_R(\tau\alpha)$	$F_R U_L$	$Q_u$ [ $\text{kWh/m}^2 \text{ year}$ ]
Selective coating (sc)	0.80	4.20	265
1-teflon film + sc	0.77	3.33	306
2-teflon films + sc	0.74	3.05	305
Corrugated-teflon film + sc	0.78	3.20	327
Arel-honeycomb + sc	0.68	2.00	340
MSA	0.74	1.43	431

- $K_{s,\lambda}$  scattering coefficient (1/m)  
 $K_{T,\lambda}$  total (i.e., scattering plus absorption) coefficient (1/m)  
 $L$  slab thickness (m)  
 $n$  number of volume elements and index of refraction  
 $s$  distance traveled in the medium (m)  
 $T$  temperature (K)  
 $T_R$  radiant temperature,  $[(T_1^2 + T_2^2)(T_1 + T_2)/4]^{1/3}$   
 $\Delta V_k$  volume of volume element  $k$  ( $m^3$ )

#### Greek

- $\epsilon_k$  emissivity of surface  $k$   
 $\theta$  angle of incidence ( $^\circ$ )  
 $\lambda$  wavelength (m)  
 $\mu$   $\cos \varphi$  where  $\varphi$  is the angle between surface normal and direction of propagation  
 $\Phi$  phase function; for Rayleigh scattering  $\Phi = \frac{3}{4} \cdot (1 + \cos^2 \varphi)$  where  $\varphi$  is the angle between the incident and scattered radiation  
 $\sigma$  Stefan-Boltzmann constant ( $5.6697 \cdot 10^{-8} \text{ W/m}^2 \text{ K}^4$ )  
 $\tau(\theta)$  angular transmittance for beam radiation  
 $\omega$  solid angle  
 $\Omega_i$  albedo for scattering in volume element  $i$

#### Subscripts

- b** beam radiation  
**d** diffuse radiation  
**sk** denotes surface  $k$   
**vk** volume element  $k$   
 $\lambda$  wavelength

#### REFERENCES

- ASHRAE Standard 93-77, *Methods of testing to determine the thermal performance of solar collectors*, ASHRAE, New York (1977).
- W. A. Beckman, Solution of heat transfer problems on a digital computer, *Solar Energy* **13**, 293-300 (1971).
- M. J. Brandemuehl and W. A. Beckman, Transmission of diffuse radiation thorough CPC and flat-plate collector glazing, *Solar Energy* **24**, 511 (1980).
- R. Caps and J. Fricke, Infrared radiation heat transfer in highly transparent silica aerogel, *Solar Energy*, **36**, 361-364 (1986).
- J. A. Duffie and W. A. Beckman, *Solar engineering of thermal processes 2nd ed.*, Wiley-Interscience Publication, New York (1991).
- D. K. Edwards, Solar absorption by each element in an absorber-coverglass array, *Solar Energy* **19**, 401-402 (1977).
- L. B. Evans, C. M. Chu, and S. W. Churchill, The effect of anisotropic scattering on radiant transport, *ASME Journal of Heat Transfer* **87**, 381-387 (1965).
- J. Fricke (ed.), *Aerogels, Spring Proceedings in Physics*, vol. 6, Springer-Verlag, New York (1986).
- H. C. Hottel and A. F. Sarofim, *Radiative transfer*, McGraw-Hill, New York (1967).
- K. I. Jensen, *Transparent cover with evacuated silica aerogel*, Thermal Insulation Laboratory, Technical University of Denmark (1989).
- S. Henning and L. Svensson, Production of silica aerogel, *Physica Scripta* **23**, 697-702 (1981).
- B. Karlsson, *Potential improvements for high temperature flat-plate collectors*, North Sun, Borlunge, Sweden (1988a).
- B. Karlsson, *Transparent insulation for high temperature flat-plate collectors*, North Sun, Borlunge, Sweden (1988b).
- B. Kellner, Erste deutsche Grossserien-Fertigung von Hochleistungs-Kollektoren, *Sonnenergie & Wärmepumpe* **14**, Heft 3 (1989).
- B. H. J. McKellar and M. A. Box, The scaling group of the radiative transfer equation, *J. Atmospheric Sciences* **38**, 1063-1068 (1981).
- M. Rubin and C. M. Lampert, Transparent silica aerogels for window insulation, *Solar Energy Material* **7**, 393-400 (1983).
- P. Scheuerpflug, R. Caps, D. Buttner, and J. Fricke, Apparent thermal conductivity of evacuated  $\text{SiO}_2$ -aerogel tiles under variation of radiative boundary conditions, *Int. J. Heat Mass Transfer* **28**, 2299-2306 (1985).
- R. Siegel and J. R. Howell, *Thermal radiation heat transfer* 2nd ed., McGraw-Hill, New York (1981).
- A. F. Souka and H. H. Safwat, Optimum orientations for the double exposure flat-plate collector and its reflectors, *Solar Energy* **10**, 170 (1966).
- S. Svendsen and K. I. Jensen, Flat-plate solar collector with monolithic silica aerogel, *Presented at the 10th ISES Solar World Congress* (Paper No. 2.2.3), Hamburg (1987).
- S. Svendsen, Solar collector based on monolithic silica aerogel, *Presented at the 11th ISES Solar World Congress*, Kobe Japan (1989).
- J. G. Symons, Calculation of the transmittance-absorptance product for flat-plate collectors with convection suppression devices, *Solar Energy* **38**, 637-640 (1984).
- P. H. Tewari, A. J. Hunt, J. G. Lieber, and K. Lofftus, Microstructural properties of transparent silica aerogels, In: *Aerogels, Spring Proceedings in Physics*, vol. 6, J. Fricke (ed.) Springer-Verlag, New York, (1986).
- R. Viskanta, Heat transfer by conduction and radiation in absorbing and scattering materials, *Trans. ASME Journal of Heat Transfer* **87**, 143-150 (1965).
- J. A. Wiebelt and J. B. Henderson, Selected ordinates for total solar radiation property evaluation from spectral data, *Trans. ASME Journal of Heat Transfer* **101**, 101-107 (1979).